JACS
JOURNAL OF THE AMERICAN CHEMICAL SOCIETY
Communication
pubs.acs.org/JACS

# Direct NMR Detection of Bifurcated Hydrogen Bonding in the α-Helix N-Caps of Ankyrin Repeat Proteins

Matthew R. Preimesberger,[†] Ananya Majumdar,[†] Tural Aksel,[†] Kevin Sforza,[†] Thomas Lectka,[‡] Doug Barrick,[†] and Juliette T. J. Lecomte*[,†]

[†]T. C. Jenkins Department of Biophysics and [‡]Department of Chemistry, Johns Hopkins University, 3400 North Charles Street, Baltimore, Maryland 21218, United States

Supporting Information

**ABSTRACT:** In biomolecules, bifurcated H-bonds typically involve the interaction of two donor protons with the two lone pairs of oxygen. Here, we present direct NMR evidence for a bifurcated H-bonding arrangement involving *nitrogen* as the acceptor atom. Specifically, the H-bond network comprises the Nδ1 atom of histidine and both the backbone N−H and side-chain Oγ-H of threonine within the conserved TXXH motif of ankyrin repeat (AR) proteins. Identification of the H-bonding partners is achieved via solution NMR H-bond scalar coupling (HBC) and H/D isotope shift experiments. Quantitative determination of $^{2h}J_{NN}$ HBCs supports that Thr N−H···Nδ1 His H-bonds within internal repeats are stronger (∼4 Hz) than in the solvent exposed C-terminal AR (∼2 Hz). In agreement, p$K_a$ values for the buried histidines bridging internal ARs are several units lower than those of the C-terminus. Quantum chemical calculations show that the relevant $^{2h}J$ and $^{1h}J$ couplings are dominated by the Fermi contact interaction. Finally, a Thr-to-Val replacement, which eliminates the Thr Oγ-H···Nδ1 His H-bond and decreases protein stability, results in a 25% increase in $^{2h}J_{NN}$, attributed to optimization of the Val N−H···Nδ1 His H-bond. Overall, the results provide new insights into the H-bonding properties of histidine, a refined structural rationalization for the folding cooperativity of AR proteins, and a challenging benchmark for the calculation of HBCs.

Hydrogen bonds (H-bonds) are essential structural elements in the self-assembly, stability, and remarkable catalytic properties of biomolecules. These low energy interactions participate in processes essential to life either singly or as intricate networks conveying structural and thermodynamic cooperativity. Yet, the presence and configuration of intramolecular H-bonds, along with their relative strength, are difficult to establish with direct experimental methods. By default, H-bonds are often modeled in crystallographic structures using theoretical idealized geometry, therefore leaving the precise configuration unknown and important instances of strained H-bonds unnoticed.

Ankyrin repeat (AR) proteins have highly cooperative folding−unfolding transitions.[1] Most of the available X-ray models show a conspicuous array of H-bonds extending from repeat to repeat.[2,3] This array involves conserved TXXH motifs initiating the first α-helix of each repeat (Figure 1).[2−4] Histidine plays an essential role within and between adjacent TXXH motifs. Specifically, a side-chain/main-chain interaction involving the His Nδ1 and Thr NH caps the N-terminus of the α-helix.[5] In addition, successive ARs pack against each other by using the Nε2H of the TXXH histidine as an H-bond donor to the carbonyl group of the residue preceding the TXXH threonine of the next repeat.[4,6] To produce the detailed description of the H-bond network necessary to rationalize thermodynamic properties, we are pursuing solution NMR studies of consensus AR proteins. Here, we provide direct evidence for stable bifurcated H-bonds in TXXH helix capping motifs and demonstrate the importance of the Thr hydroxyl group for the stability of the AR fold.

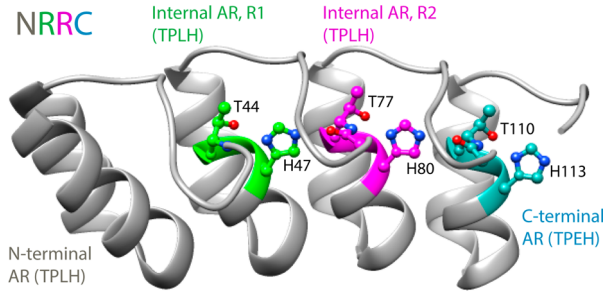


**Figure 1.** Ribbon diagram of the first four ARs in E3_19 (PDB: 2BKG) as a model for the NRRC protein discussed in this work (residue numbers correspond to NRRC). Each AR is an ∼33-residue helix-turn-helix module followed by an extended β-hairpin loop. The Thr and His of interest are shown in ball-and-stick representation (green, 2nd repeat T44−H47; magenta, 3rd repeat T77−H80; cyan, C-terminal repeat T110−H113). NRRC contains an additional N-terminal TXXH motif (T11−H14).

Amide H/D exchange rates and the response of amide $^1$H chemical shifts to temperature are routinely used to infer the presence of H-bonds in proteins.[7] These approaches are experimentally straightforward, but they do not identify acceptor atoms or report on local structure. In contrast, scalar couplings across H-bonds (HBCs)[8−13] are challenging to measure, but provide information not otherwise experimentally accessible. In particular, the magnitude of the HBC ($^{h}J$) is exquisitely sensitive to changes in bonding geometry,[14−18] which makes this

**Received:** October 20, 2014
**Published:** January 12, 2015




DOI: 10.1021/ja510784g
J. Am. Chem. Soc. 2015, 137, 1008−1011

parameter well suited for interrogation of H-bond strain and relaxation.[19]

The most common H-bond in proteins is of the N−H···O═C type and has $|^{3h}J_{NC'}|$ and $|^{2h}J_{HC'}|$ HBCs below 1 Hz.[10,13,20,21] The small $^{h}J$ values and the yet smaller variations caused by different structural contexts often limit the feasibility and utility of these measurements to relatively small proteins. However, the $^{2h}J_{NN}$ coupling constants in H-bonds of the N−H···N type can be as large as 11 Hz.[22] We therefore focused on the N−H···N$\delta$1 interaction. A survey of the Protein Data Bank indicates that the TXXH cap is found in several non-AR protein structures (Table S1). These will offer interesting opportunities for comparative studies.

In prior structural work, we assigned the backbone $^{1}$H, $^{15}$N, and $^{13}$C NMR signals of the three-repeat consensus AR protein NRC, where N refers to the N-terminal AR, R to an internal AR, and C to the C-terminal AR.[1] Here, we extend our study to the four-repeat AR protein NRRC, which contains an additional TXXH motif. From $^{1}$H−$^{15}$N LR HMQC spectra (Figure S1B,C) we deduce that each capping histidine adopts the N$\varepsilon$2H tautomer[23] in agreement with data published on the naturally occurring AR protein gankyrin.[4] Intra- and inter-repeat NOEs (Figure S2A) orient the imidazole rings as in Figure 1.

In NRC, a soft HNN-COSY experiment detects three Thr(i) N−H···N$\delta$1 His(i+3) H-bonds through $^{2h}J_{NN}$-mediated cross peaks between the NH of T11 (T44, T77) and N$\delta$1 of H14 (H47, H80) (Figure S3). In NRRC, there are four detectable signals (Figure 2a, black peaks). A complete NMR connectivity map demonstrating the helix capping Thr N−H···N$\delta$1 His H-bonds in NRRC is presented in Figure S1.

To investigate how the attributes of Thr N−H···N$\delta$1 His H-bonds vary from repeat to repeat (e.g., R1 to R2 to C in NRRC), we measured the magnitude of $^{2h}J_{NN}$ by a quantitative (Q) spin−echo difference method.[24,25] Figure 2b shows portions of Q-$^{2h}J_{NN}$ 1-D HSQC spectra collected on NRRC. The NH signals of T44, T77, and T110 undergo $^{2h}J_{NN}$ modulation with frequencies reporting on each coupling constant. Peak heights were determined as a function of the $J_{NN}$ modulation period ($\tau$) and fitted according to the relationship[25] $I(\tau) = A \cos(\pi J \tau)$ to extract $^{2h}J_{NN}$ values. In NRRC (Figure 2c), the internal TPLH H-bonds (T44−H47, T77−H80) have $^{2h}J_{NN}$ values of ~3.9−4.0 Hz, whereas the C-terminal TPEH H-bond has an attenuated value (T110−H113, ~2.1 Hz). Because of $^{1}$H overlap, only an upper bound for the N-terminal T11-H14 HBC was determined ($^{2h}J_{NN}$ < 4.1 Hz, not shown). The varying magnitude of $^{2h}J_{NN}$ from internal to terminal repeat (R1 = R2 > C) results from differences in H-bond geometry, time-averaged populations, or both. The C-terminal T110−H113 motif has high solvent exposure and no carbonyl acceptor for H113 N$\varepsilon$2-H, which likely destabilizes the N−H···N$\delta$1 bond relative to those in internal repeats. Similar differences between internal (T44−H47, $^{2h}J_{NN}$ ~4.1 Hz) and C-terminal (T77−H80, $^{2h}J_{NN}$ ~1.8 Hz) H-bonds are observed in NRC (Table 1, Figure S4A).

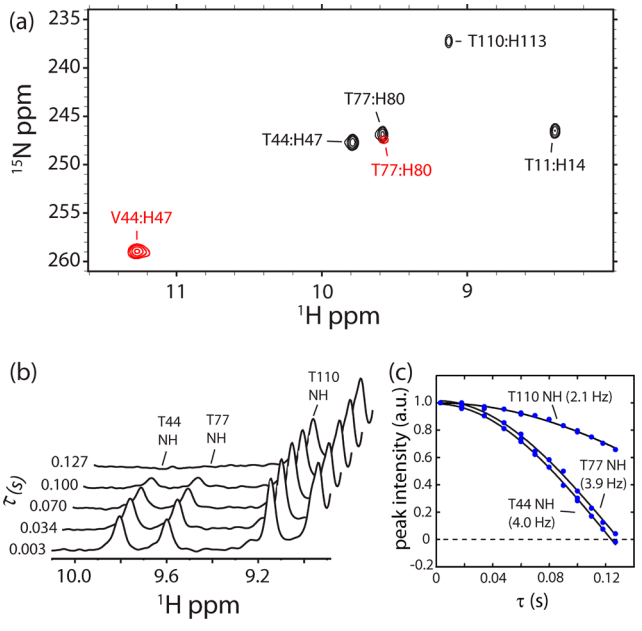


**Figure 2.** (a) Overlay of 600 MHz soft HNN-COSY spectra collected on $^{15}$N-labeled consensus AR proteins for detection of backbone N−H···N$\delta$1 histidine H-bonds: NRRC (pH 6.6, 298 K, black) and T44V NRRC (pH 7.5, 308 K, red). Labels identify NH:N$\delta$1 bonding partners. (b) Downfield region of quantitative $^{2h}J_{NN}$-modulation 1-D HSQC spectra collected on NRRC. (c) Intensity-normalized peak heights from (b) plotted as a function of the modulation period, $\tau$. Solid lines represent the best fit of the data to a cosine wave (see text).

**Table 1. Chemical Shifts, $^{2h}J_{NN}$ Coupling Constants, and $^{2h}\Delta$ $^{1}$H Isotope Shifts in AR TXXH Motifs (298 K, pH 6.6)**

| Protein and proton | H-bond partners | $\delta$ (ppm) | $\lvert^{2h}J_{NN}\rvert$ (Hz) | $^{2h}\Delta$ $^{1}$H (ppb) |
|---|---|---|---|---|
| NRC NH | T44-H47 | 9.98 | 4.1 ± 0.2 | nd[b] |
| NRC NH | T77-H80 | 9.18 | 1.8 ± 0.2 | nd[b] |
| NRRC NH | T44-H47 | 9.79 | 4.0 ± 0.2 | −53 ± 5 |
| NRRC O$\gamma$H | T44-H47 | 6.36 | | −47 ± 5 |
| NRRC NH | T77-H80 | 9.58 | 3.9 ± 0.2 | −53 ± 5 |
| NRRC O$\gamma$H | T77-H80 | 6.75 | | nd[b] |
| NRRC NH | T110-H113 | 9.13 | 2.1 ± 0.1 | nd[b] |
| T44V NH | V44-H47 | 11.27[a] | 5.2 ± 0.7[a] | 0 |
| T44V NH | T77-H80 | 9.57[a] | 3.4 ± 0.5[a] | −55 ± 5 |
| T44V O$\gamma$H | T77-H80 | 6.70[a] | | nd[b] |

[a]Data collected at 308 K, pH 7.5. Most N−H···N type H-bonds undergo thermal expansion (longer distance, lower $^{2h}J_{NN}$) with increasing temperature.[32] [b]Not determined.

The trend in $^{2h}J_{NN}$ values is mirrored in other physicochemical properties. For example, we measured the apparent p$K_a$ of each TXXH histidine within NRR, a protein containing identical repeats at internal (R1) and C-terminal (R2) positions, by following the His H$\varepsilon$1, H$\delta$2, and N$\delta$1 resonances as a function of pH (Figure S5). H47, within R1, remains in the neutral state at pH values below ~3, until the protein begins to undergo global acid unfolding. H14 of the N-terminal AR is buried and shows similar behavior. In contrast, the ionization midpoint of H80 (within R2) is only moderately depressed (apparent p$K_a$ = 5.7). Protonation of histidine necessarily breaks the N−H···N$\delta$1 H-bond, and greater p$K_a$ depression should in part result from stronger H-bonds. Therefore, the data are consistent with the use of the $^{2h}J_{NN}$ HBC as a proxy for relative H-bond strength. The difference between buried and solvent exposed N−H···N$\delta$1 H-bonds in AR repeats is analogous to the difference observed between the middle and ends of nucleic acid secondary structures, where fraying leads to smaller $^{2h}J_{NN}$ values.[16]

We next sought to detect Thr N−H···N$\delta$1 His $^{1h}J_{HN}$ HBCs in NRRC by using a high-sensitivity $^{1}$H−$^{15}$N LR HMQC approach.[23] These $^{1h}J_{HN}$ were not observed, but surprisingly, the experiment yielded $J$-correlations between T44 (T77) O$\gamma$−H


DOI: 10.1021/ja510784g
J. Am. Chem. Soc. 2015, 137, 1008−1011

and H47 (H80) Nδ1 (Figure 3a,b). LR HSQC modulation experiments (Figure S6) confirmed the buildup of the weak T44

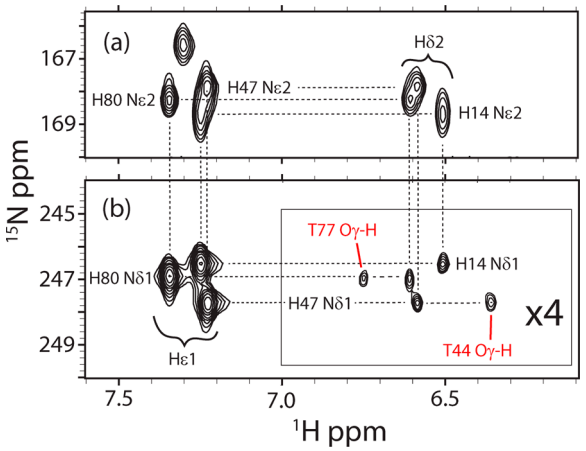


**Figure 3.** (a) Upfield and (b) downfield regions of the $^{1}H-^{15}N$ LR HMQC spectrum of NRRC at pH 6.6, 298 K. Strong $^{2}J_{NH}$ Nε2–Hε1, Nε2–Hδ2, Nδ1–Hε1, and weak $^{3}J_{NH}$ Nδ1–Hδ2 intra-imidazole correlations are indicated. The $^{1h}J_{HN}$ His Nδ1–H–Oγ Thr H-bond correlations are labeled in red.

Oγ–H···Nδ1 H47 and T77 Oγ–H···Nδ1 H80 cross peaks. From these spectra, a 3-Hz upper limit for $^{1h}J_{HN}$ was obtained, which is similar to the measured $^{1h}J_{HN}$ values of N···H–N and N···H–O H-bonds in nucleic acids.[16,21,26−28] The observation of $^{2h}J_{NN}$ and $^{1h}J_{HN}$ HBCs strongly suggests that H47 (H80) Nδ1 serves as a bifurcated H-bond acceptor to T44 (T77) N–H and Oγ–H.

An H/D exchange experiment was performed to test the proposed bifurcated H-bond scheme. When an $^{15}N$-labeled NRRC NMR sample was diluted into a 50:50 $H_2O/D_2O$ solvent mixture, we observed H/D equilibration of Thr hydroxyl groups, as illustrated by the reduction in intensity of the resolved T44 Oγ–H signal (Figure 4a,b). Interestingly, equilibration was accompanied by splitting of T44 and T77 N–H signals, confirmed with $^{1}H-^{15}N$ HSQC spectra (Figure S7A–B). We hypothesize that the population of T44 Oγ–H and Oγ–D species and relatively slow H/D exchange (<5 $s^{-1}$; see Figure S7)

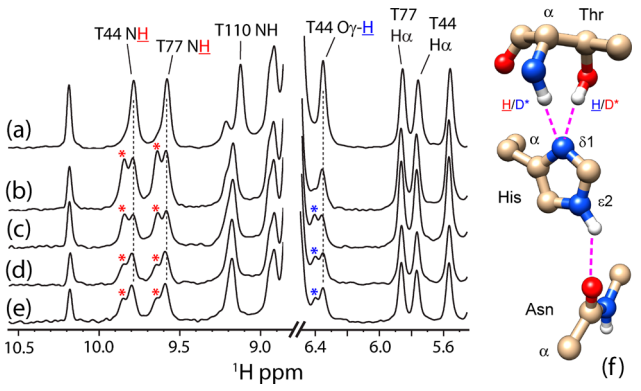


**Figure 4.** (a–e) $^{15}N$-decoupled $^{1}H$ 1-D spectra of NRRC in $H_2O/D_2O$ mixtures. (a) 90:10; (b) 50:50, 1.5 h incubation; (c) sample (b) after 24 h; (d) dilution of sample (c) to achieve a 66:34 mixture, 40 min; (e) sample (d) after 21 h. Peaks marked with * result from the presence of a D nucleus at the adjacent H-bond. (f) Proposed origin for $^{2h}\Delta$ H/D isotope effect: a bridging His acts as acceptor to both Thr amide and hydroxyl hydrogens.

cause a two-bond isotope effect, $^{2h}\Delta^{1}H = \delta^{1}H(H) - \delta^{1}H(D) = -53$ ppb, on the corresponding amide NH, communicated via shared interaction with H47 Nδ1 (Figure 4f). An identical effect on the NH of T77 ($^{2h}\Delta^{1}H = -53$ ppb) is attributed to the population and slow exchange of T77 Oγ–H/D species. H/D isotope shifts were not observed for any other backbone amide. However, a reciprocal isotope shift (splitting of Thr Oγ–H signal caused by mixed H/D occupancy at the Thr amide) is detected after ∼24 h (Figure 4c). The $^{2h}\Delta^{1}H$ value is −47 ppb for T44 OγH. Further variation in the solvent composition confirms the assignment of each isotopomer (Figure 4d–e). The N–H···Nδ1···H–Oγ two-bond isotope effects observed for consensus ARs are of greater magnitude than those reported for protein N–H···O···H–N H-bonds ($^{2h}\Delta^{1}H = -18$ to +23 ppb),[29] but are significantly smaller than those detected for O–H···O···H–O H-bonds in the oxyanion hole of ketosteroid isomerase ($^{2h}\Delta^{1}H = -250$ to −170 ppb).[30] The two-bond isotope shifts ($^{2h}\Delta^{1}H$) and HBCs ($^{2h}J_{NN}$ and $^{1h}J_{HN}$) in NRRC provide independent evidence for bifurcated H-bonding in the α-helix N-cap TXXH motif.

The consequences of Thr Oγ–H···Nδ1 His H-bond deletion were explored with the isosteric T44V replacement in NRRC. We reasoned that elimination of the bifurcated N–H···Nδ1···H–Oγ interaction would perturb the remaining N–H···Nδ1 His H-bond. Denaturation experiments conducted at pH 8.0 indicate that T44V NRRC is destabilized by ∼2.6 kcal/mol relative to the consensus protein (Figure S8). Figure 2a shows the HNN-COSY spectrum of the variant (red peaks). H-bond detection in T44V NRRC is difficult because of protein aggregation at concentrations above ∼100 μM; nevertheless, the weak T77 N–H···Nδ1 H80 correlation is observable and overlays well with the reference NRRC signal. In contrast, the V44 N–H···Nδ1 H47 cross peak has increased intensity compared to the reference T44 N–H···Nδ1 H47 cross peak. Also remarkable are the large downfield shifts of both V44 amide $^{1}H$ (∼1.5 ppm) and H47 $^{15}N\delta1$ (∼10 ppm) (Figures 2a and S9), signifying N–H···N H-bond reconfiguration and a decrease in bond length.[14,16,27,29,30]

Measurement of $^{2h}J_{NN}$ due to the V44-H47 (∼5.2 Hz) and T77-H80 (∼3.4 Hz) H-bonds provides insight into the repercussions of the T44V replacement relative to the TPLH helix caps in NRRC. In the T44-H47 and T77-H80 bifurcated interactions, the $^{2h}J_{NN}$, $^{1h}J_{HN}$, and $^{2h}\Delta^{1}H$ isotope shift data support that the His ring orients its Nδ1 atom between Thr NH and OγH, adopting a nonlinear geometry for both H-bonds and leading to relatively small T44-H47 and T77-H80 N–H···Nδ1 $^{2h}J_{NN}$ couplings (∼4 Hz). Upon T44V replacement, the observed ∼25% increase in $^{2h}J_{NN}$ (Figure S4B,C) suggests a straightening (and concomitant shortening) of the Val N–H···Nδ1 His H-bond.

To gain insight into the nature of the N–H···Nδ1···H–Oγ H-bond network, quantum chemical calculations (described in the Supporting Information) were performed using Gaussian 09[31] on fragments of 2BKG mimicking an internal repeat. Energy minimization from multiple starting geometries (Figure S10) validated the use of the X-ray coordinates for the calculations. The computed HBCs (Figure S11, Table S2) are $^{2h}J_{NN} = +3.0$ Hz, $^{1h}J_{HN} = +2.0$ Hz (N–H···Nδ1), and $^{1h}J_{HN} = +2.2$ Hz (Nδ1···H–Oγ), all dominated by the Fermi contact (FC) contribution. These values are in reasonable agreement with the experimental numbers. Along with the geometry of the TXXH unit, the HBCs suggest that the His Nδ1 $sp^2$ lone pair is the major contributor to both hydrogen bonds. H-bonding may also be augmented by interaction with the His π-system, as in a cation–π interaction.[33] The larger $^{2h}J_{NN}$ in T44V NRRC is consistent with a


DOI: 10.1021/ja510784g
J. Am. Chem. Soc. 2015, 137, 1008−1011

repositioning of the histidine ring that improves the orbital overlap and enhances the FC effect[34] (Figure S12, Table S2).

Collectively, the data illuminate a relationship between the magnitude of $^{2h}J_{NN}$ scalar couplings and H-bond sharing. The N−H···N HBCs measured for bifurcated H-bonds in buried consensus ARs (∼4 Hz) are significantly smaller than those for the few other reported protein N−H···N HBCs (∼6−11 Hz),[22,35,36] an indication of weaker bonds and nonideal geometry in the former. Stability compensation is likely provided by the bifurcated arrangement. Importantly, our description of the H-bond network clarifies the role of the threonine hydroxyl group and contributes a comparative view of the TXXH motif within individual repeats. Further work will extend to longer AR proteins in order to explore the generality of the bifurcated N−H···N$\delta$1···H−O$\gamma$ H-bond and determine the factors controlling its formation.

## ■ ASSOCIATED CONTENT

### Supporting Information

Sample preparation; PDB survey results; NMR information; HSQC, LR HMQC, HNN-COSY NRRC spectra; HNN-COSY NRC spectra; NRRC His N$\epsilon$2H NOEs, $^{2h}J_{NN}$ modulation curves; NRR His p$K_a$ determination, NRRC LR HSQC spectra, $^{2h}\Delta^{1}$H isotope shifts (NRRC HSQC), NRRC and T44V denaturation curves; T44V NRRC HSQC, LR HMQC, HNN-COSY spectra; computational results. This material is available free of charge via the Internet at http://pubs.acs.org.

## ■ AUTHOR INFORMATION


### Corresponding Author

*lecomte_jtj@jhu.edu


### Notes

The authors declare no competing financial interest.

## ■ ACKNOWLEDGMENTS

Financial support was provided by NSF MCB-0843439 to J.T.J.L., NIH R01-GM-068462 to D.B., T32-GM-008403 for M.R.P., and T32-GM-007231 for K.S. The authors thank George Rose and Christopher Falzone for helpful discussions.

## ■ REFERENCES


(1) Aksel, T.; Majumdar, A.; Barrick, D. *Structure* **2011**, *19*, 349.
(2) Kohl, A.; Binz, H. K.; Forrer, P.; Stumpp, M. T.; Pluckthun, A.; Grutter, M. G. *Proc. Natl. Acad. Sci. U.S.A.* **2003**, *100*, 1700.
(3) Binz, H. K.; Kohl, A.; Pluckthun, A.; Grutter, M. G. *Proteins* **2006**, *65*, 280.
(4) Yuan, C. H.; Li, J. N.; Mahajan, A.; Poi, M. J.; Byeon, I. J. L.; Tsai, M. D. T. *Biochemistry* **2004**, *43*, 12152.
(5) Aurora, R.; Rose, G. D. *Protein Sci.* **1998**, *7*, 21.
(6) Guo, Y.; Yuan, C. H.; Tian, F.; Huang, K.; Weghorst, C. M.; Tsai, M. D.; Li, J. N. *J. Mol. Biol.* **2010**, *399*, 168.
(7) Baxter, N. J.; Williamson, M. P. *J. Biomol. NMR* **1997**, *9*, 359.
(8) Blake, P. R.; Lee, B.; Summers, M. F.; Adams, M. W.; Park, J. B.; Zhou, Z. H.; Bax, A. *J. Biomol. NMR* **1992**, *2*, 527.
(9) Dingley, A. J.; Grzesiek, S. *J. Am. Chem. Soc.* **1998**, *120*, 8293.
(10) Cornilescu, G.; Hu, J. S.; Bax, A. *J. Am. Chem. Soc.* **1999**, *121*, 2949.
(11) Hennig, M.; Williamson, J. R. *Nucleic Acids Res.* **2000**, *28*, 1585.
(12) Majumdar, A.; Kettani, A.; Skripkin, E.; Patel, D. J. *J. Biomol. NMR* **1999**, *15*, 207.
(13) Liu, A. Z.; Hu, W. D.; Majumdar, A.; Rosen, M. K.; Patel, D. J. *J. Biomol. NMR* **2000**, *17*, 305.
(14) Heinz, T.; Moreira, O.; Pervushin, K. *Helv. Chim. Acta* **2002**, *85*, 3984.
(15) Barfield, M.; Dingley, A. J.; Feigon, J.; Grzesiek, S. *J. Am. Chem. Soc.* **2001**, *123*, 4014.
(16) Dingley, A. J.; Masse, J. E.; Peterson, R. D.; Barfield, M.; Feigon, J.; Grzesiek, S. *J. Am. Chem. Soc.* **1999**, *121*, 6019.
(17) Barfield, M. *J. Am. Chem. Soc.* **2002**, *124*, 4158.
(18) Grzesiek, S.; Cordier, F.; Jaravine, V.; Barfield, M. *Prog. Nucl. Magn. Reson. Spectrosc.* **2004**, *45*, 275.
(19) Cordier, F.; Wang, C.; Grzesiek, S.; Nicholson, L. K. *J. Mol. Biol.* **2000**, *304*, 497.
(20) Cornilescu, G.; Ramirez, B. E.; Frank, M. K.; Clore, G. M.; Gronenborn, A. M.; Bax, A. *J. Am. Chem. Soc.* **1999**, *121*, 6275.
(21) Alkorta, I.; Elguero, J.; Denisov, G. S. *Magn. Reson. Chem.* **2008**, *46*, 599.
(22) Hennig, M.; Geierstanger, B. H. *J. Am. Chem. Soc.* **1999**, *121*, 5123.
(23) Pelton, J. G.; Torchia, D. A.; Meadow, N. D.; Roseman, S. *Protein Sci.* **1993**, *2*, 543.
(24) Majumdar, A.; Kettani, A.; Skripkin, E. *J. Biomol. NMR* **1999**, *14*, 67.
(25) Bax, A.; Vuister, G. W.; Grzesiek, S.; Delaglio, F.; Wang, A. C.; Tschudin, R.; Zhu, G. *Methods Enzymol.* **1994**, *239*, 79.
(26) Pervushin, K.; Ono, A.; Fernandez, C.; Szyperski, T.; Kainosho, M.; Wüthrich, K. *Proc. Natl. Acad. Sci. U.S.A.* **1998**, *95*, 14147.
(27) Benedict, H.; Shenderovich, I. G.; Malkina, O. L.; Malkin, V. G.; Denisov, G. S.; Golubev, N. S.; Limbach, H. H. *J. Am. Chem. Soc.* **2000**, *122*, 1979.
(28) Giedroc, D. P.; Cornish, P. V.; Hennig, M. *J. Am. Chem. Soc.* **2003**, *125*, 4676.
(29) Pietrzak, M.; Try, A. C.; Andrioletti, B.; Sessler, J. L.; Anzenbacher, P., Jr.; Limbach, H. H. *Angew. Chem., Int. Ed.* **2008**, *47*, 1123.
(30) Del Bene, J. E.; Bartlett, R. J. *J. Am. Chem. Soc.* **2000**, *122*, 10480.
(31) Frisch, M. J.; Trucks, G. W.; Schlegel, H. B.; Scuseria, G. E.; Robb, M. A.; Cheeseman, J. R.; Scalmani, G.; Barone, V.; Mennucci, B.; Petersson, G. A.; Nakatsuji, H.; Caricato, M.; Li, X.; Hratchian, H. P.; Izmaylov, A. F.; Bloino, J.; Zheng, G.; Sonnenberg, J. L.; Hada, M.; Ehara, M.; Toyota, K.; Fukuda, R.; Hasegawa, J.; Ishida, M.; Nakajima, T.; Honda, Y.; Kitao, O.; Nakai, H.; Vreven, T.; Montgomery, J. A., Jr.; Peralta, J. E.; Ogliaro, F.; Bearpark, M. J.; Heyd, J.; Brothers, E. N.; Kudin, K. N.; Staroverov, V. N.; Kobayashi, R.; Normand, J.; Raghavachari, K.; Rendell, A. P.; Burant, J. C.; Iyengar, S. S.; Tomasi, J.; Cossi, M.; Rega, N.; Millam, N. J.; Klene, M.; Knox, J. E.; Cross, J. B.; Bakken, V.; Adamo, C.; Jaramillo, J.; Gomperts, R.; Stratmann, R. E.; Yazyev, O.; Austin, A. J.; Cammi, R.; Pomelli, C.; Ochterski, J. W.; Martin, R. L.; Morokuma, K.; Zakrzewski, V. G.; Voth, G. A.; Salvador, P.; Dannenberg, J. J.; Dapprich, S.; Daniels, A. D.; Farkas, Ö.; Foresman, J. B.; Ortiz, J. V.; Cioslowski, J.; Fox, D. J. *Gaussian 09*; Gaussian, Inc.: Wallingford, CT, USA, 2009.
(32) Dingley, A. J.; Peterson, R. D.; Grzesiek, S.; Feigon, J. *J. Am. Chem. Soc.* **2005**, *127*, 14466.
(33) Gallivan, J. P.; Dougherty, D. A. *Proc. Natl. Acad. Sci. U.S.A.* **1999**, *96*, 9459.
(34) Del Bene, J. E.; Perera, S. A.; Bartlett, R. J. *Magn. Reson. Chem.* **2001**, *39*, S109.
(35) Eletsky, A.; Heinz, T.; Moreira, O.; Kienhofer, A.; Hilvert, D.; Pervushin, K. *J. Biomol. NMR* **2002**, *24*, 31.
(36) Liu, A. Z.; Majumdar, A.; Jiang, F.; Chernichenko, N.; Skripkin, E.; Patel, D. J. *J. Am. Chem. Soc.* **2000**, *122*, 11226.




DOI: 10.1021/ja510784g
*J. Am. Chem. Soc.* 2015, 137, 1008−1011